# Manipulating light polarization with ultrathin plasmonic metasurfaces

Yang Zhao and Andrea Alù*

*Department of Electrical and Computer Engineering, The University of Texas at Austin, 1 University Station C0803, Austin, TX 78712, USA*

(Received 2 July 2011; revised manuscript received 4 October 2011; published 16 November 2011)

We analyze the design of ultrathin quarter-wave plates based on plasmonic metasurfaces. After exploring the general theoretical possibilities offered by thin surfaces to manipulate the impinging polarization, we propose optimal designs to realize quarter-wave metasurface plates, analyzing their frequency and angular response. Our designs may provide a large degree of linear polarization output for circularly polarized input over a broad bandwidth in the optical regime. The geometry may be implemented within currently available lithographic techniques and easily integrated with other optical devices for polarization manipulation, detection, and sensing at the nanoscale.

DOI: 10.1103/PhysRevB.84.205428 PACS number(s): 42.25.Bs, 42.25.Ja, 78.67.−n

## I. INTRODUCTION

The capability of manipulating the polarization state of light is of central interest in a variety of optical applications due to the fact that many phenomena in the visible spectrum are inherently polarization sensitive. In particular, the possibility of creating and detecting circular polarization may be of interest for advanced optical signaling and sensors due to its inherent robustness to scattering and diffraction. Currently, circular polarizers and sensors may be realized using anisotropic or chiral devices,[1] but with specific thickness limitations and quite bulky configurations. Integrating these polarizers within an ultrathin device may be of great interest in order to combine circular polarization information with nanophotonic devices and advanced sensors.[2] In this regard, recent progress in plasmonics can provide unprecedented opportunities to manipulate light polarization at the nanoscale by exploiting the strong field localization and enhancement due to the localized light interaction with surface plasmons.[3] Recent results have shown that crossed resonant plasmonic nanoantennas,[4–6] corrugated elliptical gratings,[7] patterned metallic films,[8–10] planar chiral structures,[11,12] and three-dimensional metamaterials[13] may indeed provide strong manipulation of polarization, with clear advances over currently available technology in terms of required thickness and/or bandwidth of operation. In this paper, we analyze in detail the potentials of plasmonic metasurfaces to manipulate the light polarization state, and we discuss the specific design and optimization of ultrathin quarter-wave plasmonic plates. We propose two complementary designs based on orthogonally patterned nanorods and a specifically tailored form of anisotropy that introduces a phase shift of $\pi/2$ between two orthogonal polarizations at the operating wavelength. This concept is realized by detuning the resonance of each nanorod by varying the individual aspect ratio, in a fashion similar to that proposed in recent papers.[5,6,9] Since the phase of the scattered fields sharply varies with frequency around the nanorod resonance, it is possible to tailor the phase shift between the scattered waves of two orthogonal nanorods by slightly changing their relative length around the resonant one. We analyze with full-wave simulations the overall angular and bandwidth performance of arrays of such inclusions, highlighting their optimal performance properties and their advantages in terms of lithographic realization and integration with sensors and other related technology. In the following, we present an extensive analysis of the physical mechanism behind this operation and perspectives on its potential application for practical quarter-wave plates.

## II. THEORETICAL FORMULATION

Consider an ultrathin, arbitrary planar metasurface with subwavelength thickness $d \ll \lambda_0$ placed on the plane $z = 0$. We can define the general transmission matrix $\underline{\mathbf{T}}$, describing the complex amplitudes of transmitted waves,

$$\underline{\mathbf{T}} = \begin{pmatrix} T_{xx} & T_{xy} \\ T_{yx} & T_{yy} \end{pmatrix}, \tag{1}$$

where the arbitrary element $T_{lm}$ represents the complex amplitude of the transmitted wave, linearly polarized in the $l$ direction for excitation in the $m$ direction. We assume an $e^{-i\omega t}$ time-harmonic dependence, and for simplicity we focus in (1) on normal incidence illumination.

For a metasurface period sufficiently smaller than the wavelength so that only the zeroth diffraction order can propagate away from the $xy$ plane, we can describe the metasurface with its average surface admittance $\underline{\mathbf{Y}}_\mathbf{s} = Y_{xx}\hat{\mathbf{x}}\hat{\mathbf{x}} + Y_{xy}\hat{\mathbf{x}}\hat{\mathbf{y}} + Y_{yx}\hat{\mathbf{y}}\hat{\mathbf{x}} + Y_{yy}\hat{\mathbf{y}}\hat{\mathbf{y}}$, which relates the averaged electric field to the induced electric polarization current density $\mathbf{J}_{\rm av} = \underline{\mathbf{Y}}_\mathbf{s} \cdot \mathbf{E}_{\rm av}$. We can neglect magnetic effects for excitation at normal incidence since the metasurface has negligible thickness.[14–18] By matching the boundary conditions on the metasurface, it is possible to relate the surface admittance tensor to $\underline{\mathbf{T}}$:[15,18]

$$\underline{\mathbf{Y}}_s = -\frac{2}{\eta_0}\begin{pmatrix} 1+\frac{T_{yy}}{(T_{xy}T_{yx}-T_{xx}T_{yy})} & \frac{-T_{xy}}{(T_{xy}T_{yx}-T_{xx}T_{yy})} \\ \frac{-T_{yx}}{(T_{xy}T_{yx}-T_{xx}T_{yy})} & 1+\frac{T_{xx}}{(T_{xy}T_{yx}-T_{xx}T_{yy})} \end{pmatrix}. \tag{2}$$

Equation (2) relates the surface admittance to its transmission properties, allowing its design for the specific functionality of interest. The admittance can be used as a building block in a more complex nanocircuit[19,20] or to tailor and manipulate the impinging signal. Here we explore the fundamental limits in manipulating the polarization state of impinging light, with special interest in circular polarization.

 

In the most general case, the transmission matrix (1) may be written in a circularly polarized base:

$$\underline{\mathbf{T}}_{CP} = \begin{pmatrix} T_{LL} & T_{LR} \\ T_{RL} & T_{RR} \end{pmatrix} = \begin{pmatrix} \frac{T_{xx}+T_{yy}+i(T_{xy}-T_{yx})}{2} & \frac{T_{xx}-T_{yy}-i(T_{xy}+T_{yx})}{2} \\ \frac{T_{xx}-T_{yy}+i(T_{xy}+T_{yx})}{2} & \frac{T_{xx}+T_{yy}-i(T_{xy}-T_{yx})}{2} \end{pmatrix}, \quad (3)$$

where, similar to the notation in (1), $T_{LR}$ denotes the transmission coefficient for left-handed circularly polarized (LCP) waves for right-handed circularly polarized (RCP) illumination, with similar definitions for all the other elements. Using (2), we can write $\underline{\mathbf{T}}_{CP}$ in terms of the surface admittance, and it is easy to verify that $|T_{LL}| = |T_{RR}|$ for any lossless metasurface made of reciprocal materials, as $T_{xy} = T_{yx}$ for normal incidence. By introducing absorption it may be possible to relax this constraint and introduce small circular dichroism that may distinguish between the two circular polarizations,[21] but this phenomenon has limited bandwidth and practical application. Similarly, by exciting at oblique incidence, we may be able to introduce an effective nonreciprocal response, associated with the inclusion bianisotropy.[22,23] It may be shown, in fact, that a possible inclusion asymmetry may produce a magnetoelectric coupling effect that allows $T_{xy} \neq T_{yx}$, introducing a difference between LCP and RCP responses for a single metasurface.[24] For an ultrathin surface, however, this effect may be obtained only for oblique incidence, which effectively breaks the two-dimensional (2D) symmetry of an ultrathin surface. Usually, these effects are weak and difficult to exploit in a practical configuration due to their narrow bandwidth. For these reasons, we focus in the following on manipulating the *phase difference* between $T_{LL}$ and $T_{RR}$, rather than their amplitudes, to effectively realize ultrathin quarter-wave plates, similar to a birefringent crystal but over a negligible thickness. This operation may be obtained without cross-coupling terms in $\underline{\mathbf{T}}$, i.e., for $T_{xy} = T_{yx} = 0$ in a suitably chosen reference system.

A birefringent crystal manipulates the state of polarization by introducing a phase delay of one linearly polarized component of the impinging field over the other. At the exit of the crystal, if the cumulative phase difference is exactly 90°, LCP and RCP inputs will result in linear orthogonal polarizations. We aim at designing a metasurface operating in the same way but over a single ultrathin surface. The required transmission matrix

$$\underline{\mathbf{T}} = \begin{pmatrix} \tau & 0 \\ 0 & \pm i\tau \end{pmatrix}$$

may be obtained with a surface admittance tensor (2):

$$\underline{\mathbf{Y}}_s = \begin{pmatrix} \frac{2}{\eta_0}\frac{1-\tau}{\tau} & 0 \\ 0 & \frac{2}{\eta_0}\frac{\mp i-\tau}{\tau} \end{pmatrix}, \quad (4)$$

where $\tau$ is a complex quantity $\tau = re^{i\theta}$.

In the limit of small absorption, the real part of the diagonal elements in (4) is zero, which may be obtained only when $\theta = \mp\frac{\pi}{4}$ and $r = \frac{\sqrt{2}}{2}$, i.e.,

$$\underline{\mathbf{Y}}_s = \frac{2}{\eta_0}\begin{pmatrix} \pm i & 0 \\ 0 & \mp i \end{pmatrix}, \quad (5)$$

and the corresponding transmission matrix coincides with the Jones matrix of a lossless quarter-wave plate. We also notice that the continuity of the electric and magnetic fields on an ideally thin metasurface require that the reflection matrix satisfies $\underline{\mathbf{R}} = \underline{\mathbf{T}} - \underline{\mathbf{I}} = -\underline{\mathbf{T}}^T$, where $\underline{\mathbf{I}}$ is the identity matrix and the superscript $T$ indicates the transpose operation.[25] This implies that, when Eq. (5) is satisfied, the metasurface reflection matrix also satisfies similar quarter-wave plate conditions and the total transmitted power is half of the impinging one. This will be particularly relevant in the next section, where we consider complementary plasmonic metasurfaces. In the following, we aim at realizing a plasmonic metasurface with an admittance tensor given by (5), which realizes a transmission matrix equivalent to a lossless quarter-wave plate but in an ultrathin geometry.

## III. PLASMONIC METASURFACE DESIGN

The ideal quarter-wave plate response (5) may be obtained by considering a metasurface with two orthogonal symmetry axes. Nanocrosses have been proposed to locally convert linear to circular polarization,[4] and arrays of orthogonal nanoslits have been recently suggested to realize ultrathin wave plates.[5] We explore in this context plasmonic inclusions to realize the optimal local impedance response (5) using orthogonal arrays of nanorods or nanoslits that are slightly off resonance. An ideal lossless metasurface made of nanoslits in a plasmonic thin screen provides identically zero reflection and total transmission at resonance, with a transmission phase that rapidly switches from 90° to 270° around this resonance. If we interleave two arrays of orthogonal nanoslits, one operating slightly *above* and one slightly *below* their resonance, as recently suggested in Ref. 5, we may achieve a precise 90° phase shift between the two transmitted waves. We aim here at tuning the length of the nanoslits to satisfy as closely as possible Eq. (5), both in amplitude and phase at the design wavelength $\lambda_0 = 650$ nm.

We have used full-wave numerical simulations based on a finite-integration technique[26] to realize this optimal condition in the geometry shown in Fig. 1 and to verify its wave-plate

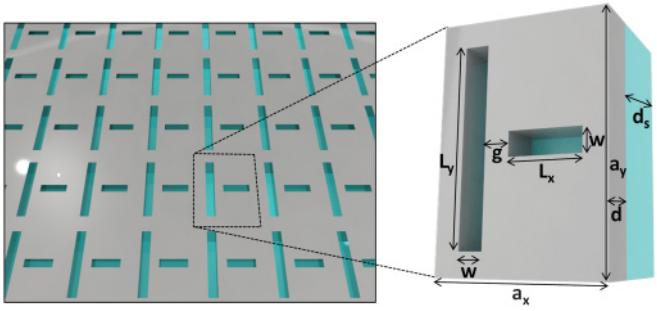


FIG. 1. (Color online) Nanoslit plasmonic metasurface, its unit cell, and the corresponding geometrical parameters.

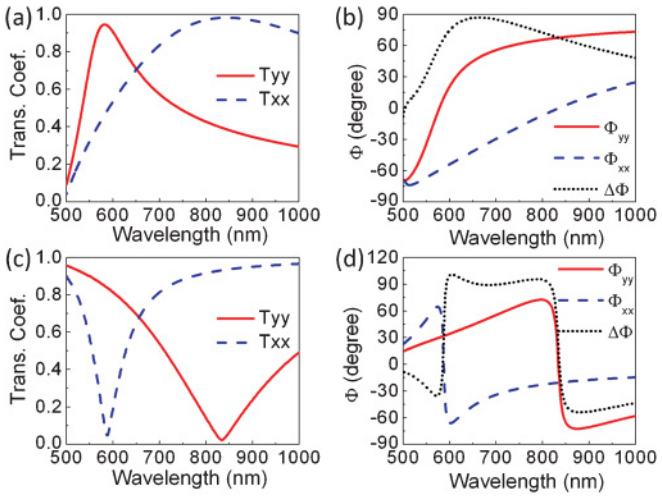


FIG. 2. (Color online) (a) Amplitude and (b) phase of the transmission coefficients for linearly polarized excitations for the optimized metasurface geometry of Fig. 1. (c, d) Similar plots for the complementary geometry, composed of plasmonic nanorods.

operation. We assume in our simulations a silver permittivity following the Drude model $\varepsilon_{\mathrm{Ag}} = \varepsilon_0(\varepsilon_\infty - \frac{f_p^2}{f(f-i\gamma)})$, with $\varepsilon_\infty = 5$, $f_p = 2.175$ PHz, and $\gamma = 4.35$ THz.[27] Each optimized unit cell is formed by two orthogonal rectangular nanoslits with a separation gap $g = 10$ nm, a vertical arm length $L_y = 160$ nm, and a lateral arm length $L_x = 60$ nm. Both nanoslits have a width $w = 20$ nm, and the screen thickness is $d = 40$ nm. The lattice constants are $a_x = 100$ nm and $a_y = 180$ nm. This configuration may be experimentally realized by evaporating a thin silver film and then applying e-beam lithography followed by reactive ion etching or by directly writing using a focused ion beam. For now, we do not consider the presence of a substrate in our design, which may be required in its practical realization ($d_s = 0$). We will consider its effects in the following.

As shown in Fig. 2(a), this optimized metasurface shows two distinct resonances when illuminated with orthogonal linear polarizations aligned along the nanoslits. At the design wavelength, the two nonzero diagonal terms of the transmission matrix have the same amplitude, $|T_{xx}| = |T_{yy}| \simeq \frac{\sqrt{2}}{2}$, and a phase difference [Fig. 2(b)] exactly equal to 90°, ensuring that its operation as an ideal ultrathin low-loss quarter-wave plate is obtained. Even though silver has some absorption in the visible spectrum, the transmission amplitudes satisfy very closely the requirements of a lossless quarter-wave plate. Indeed, we verify in Fig. 3(c) that the absorption effects are minimal over the whole frequency range of interest, and the transmittance and reflectance spectra are close to 50%.

As noticed above, we may also consider the complementary geometry formed by interleaved arrays of plasmonic nanorods. Applying Babinet's principle[28] properly extended to plasmonic screens,[29,30] we expect that the transmission properties of a complementary array of silver nanorods with same design parameters as in Fig. 2 may be approximately equal to the reflection matrix of the nanoslit array $\underline{\mathbf{R}} = -\underline{\mathbf{T}}^T$ at the design wavelength. Since $-\underline{\mathbf{T}}^T$ also satisfies the ideal quarter-wave plate conditions, the complementary design may provide a similar optical response. Because silver has finite conductivity, we do not achieve an exact complementary response, but we have verified that by slightly modifying the design of the complementary array ($L_y = 140$ nm, $L_x = 65$ nm), we achieve the quarter-wave plate condition at the design wavelength of 650 nm. The corresponding results are shown in Figs. 2(c) and 2(d), which indeed show complementary transmission properties compared to the nanoslit geometry and identical response at the design wavelength.

Figure 3 shows the amplitude and phase of the transmitted fields and the total transmission, reflection, and absorption spectra for circularly polarized inputs in both designs. Figures 3(a), 3(b), and 3(c) refer to the nanoslit metasurface, while Figs. 3(d), 3(e), and 3(f) refer to the complementary nanorod metasurface. It is seen that, as predicted, $|T_{LL}| = |T_{RR}|$ at all frequencies and both metasurfaces realize the

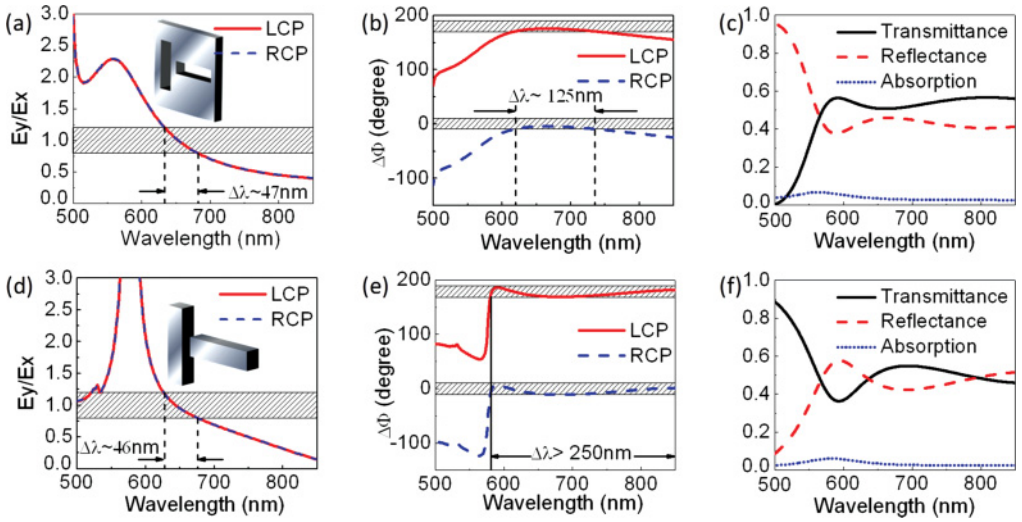


FIG. 3. (Color online) Amplitude and phase of the transmitted fields for circularly polarized excitations. (a) Amplitude ratio of transmitted $E_y/E_x$ for LCP and RCP excitation for the nanoslit metasurface of Fig. 1, (b) phase difference between $E_y$ and $E_x$, (c) transmittance, reflection, and absorption spectra for the nanoslit metasurface, and (d, e, f) similar plots for the complementary nanorod metasurface.

desired transmission conditions, in both amplitude and phase, around the same design wavelength. Due to frequency dispersion, the ideal quarter-wave plate conditions can be met only at a single wavelength, at the point of intersection of the transmission curves in Fig. 2. However, when the ratio of linearly polarized components of the transmitted wave is within the range 0.8–1.2, as shown in the shadowed region in Figs. 3(a) and 3(c), the performance as a quarter-wave plate is still acceptable. We define the wavelength range over which this condition is met the *amplitude bandwidth* of the given metasurface. Figs. 3(b) and 3(e) show the phase difference of the transmitted linearly polarized components. It is found that an acceptable range is $\pm 10^\circ$ for RCP and $170^\circ$–$190^\circ$ for LCP, as indicated by the shadowed regions in Fig. 3(b) and 3(d), which defines the metasurface *phase bandwidth*. The quarter-wave plate bandwidth of operation of the metasurface generally coincides with the minimum between these two bandwidths, but as detailed in the following, for specific operations one of the two bandwidths may be more relevant and may dominate the response.

A good figure of merit to analyze the performance of these metasurfaces, in particular for the integration with polarization imaging sensors, is represented by their degree of linear polarizaiton (DOLP), defined as $\frac{\sqrt{S_1^2+S_2^2}}{S_0}$, with $S_0, S_1,$ and $S_2$ being the Stokes parameters. This quantity effectively represents how linearly polarized the transmitted wave is for circularly polarized inputs. In this case, the *phase bandwidth* is evidently more relevant since we are not concerned about the specific direction of linear polarization output.

Figure 4 shows the DOLP of both the nanoslit and nanorod metasurfaces. The bandwdith over which the DOLP is nearly unity closely corresponds to the phase bandwdith shown in Fig. 3, which is significantly broad considered the ultrathin features of the device. We have also calculated the angle of polarization of the transmitted wave within the bandwidth in which DOLP is near unity, as shown in Figs. 4(a) and 4(b). At the design frequency, as expected, both designs provide linear polarization at 45°, but this angle changes within the bandwidth of operation due to the dispersion of $|T_{xx}|/|T_{yy}|$. For the nanoslit metasurface, we obtain linearly polarized transnmission at an angle ranging from 28° to 55° with respect to the $x$ axis within the bandwidth of interest (616–746 nm); with the nanorod metasurface the angle of linear polarization (AOLP) varies from 1° to 86° within the broader range 573–934 nm. The nanorod metasurface ensures a broader phase bandwidth and a correspondingly larger range over which the DOLP is unity, which spans almost the entire visible spectrum. Using the reciprocity theorem, we expect to obtain circularly polarized output with linearly polarized input at the AOLP indicated in Figs. 4(a) and 4(b). For this dual operation, the amplitude bandwidth is relevant since the fast and slow axes of the quarter-wave plate metasurface effectively rotate with the wavelength of operation and are not necessarily aligned with the rods or slits.

An additional relevant aspect to consider for these ultrathin designs is their robustness to variations in incidence angle, as we investigate in Figs. 4(c) and 4(d). In particular, we show the DOLP for incidence angles varying from 10° to 80° for both nanoslit and nanorod metasurfaces when RCP light impinges on the surface. For incidence angles up to 40°, a relatively large bandwidth with unity DOLP is obtained; as the incidence angle increases further, the bandwidth of operation decreases due to the occurrence of resonance dips caused by the coupling with long-range surface plasmons.[31]

In reality, a supporting substrate needs to be taken into account for the practical realization of these devices. By adding a nondispersive silicon dioxide substrate, with relative permittivity of 2.25, the inclusion resonance is shifted to longer wavelengths,[32] so the optimal design needs to take into account its influence. In Fig. 5 we show how the previous results are affected by such a glass substrate by keeping the design unchanged. First, it is observed that the quarter-wave plate operation is shifted to the longer wavelength of 704 nm. In addition, the functionality is no longer ideal since the phase relation between the two orthogonal linearly polarized transmitted waves is slightly changed, as the two transmission

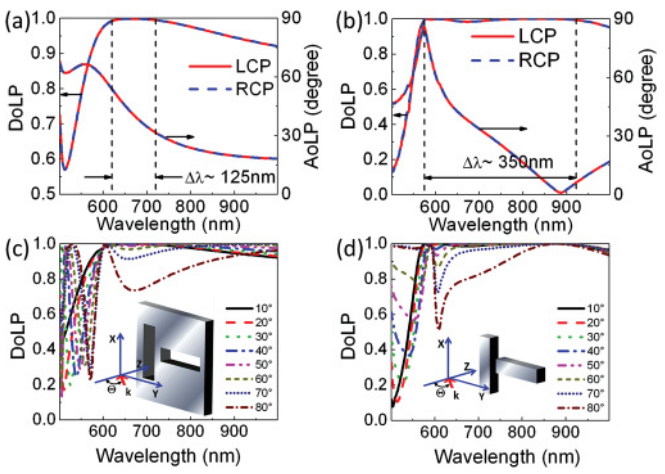


FIG. 4. (Color online) Degree of linear polarization for (a) nanoslit and (b) nanorod metasurfaces for RCP and LCP excitation and (c, d) similar plots for oblique incidence and RCP excitation. (a) and (b) show also the corresponding angle of linear polarization.

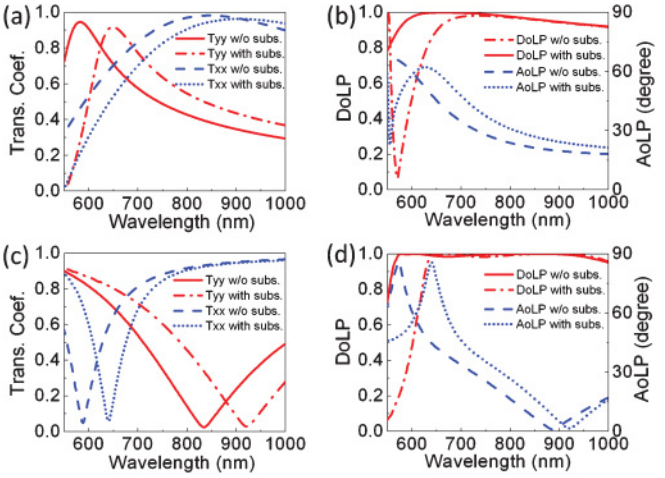


FIG. 5. (Color online) Comparison of (a) transmission coefficients and (b) DOLP for the metasurfaces made of slit inclusions, with and without the presence of a substrate, and (c, d) the same for dipole inclusions.

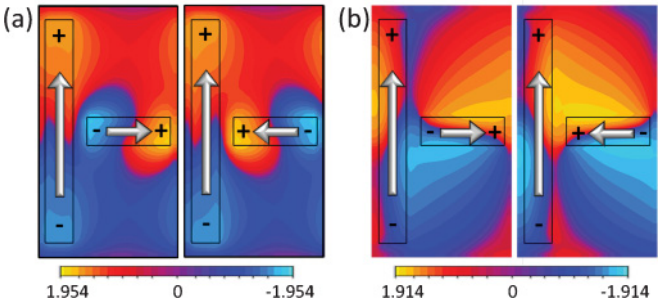


FIG. 6. (Color online) Normalized normal component of the magnetic field distribution (snapshot in time) at the metasurface output for (a) nanoslit and (b) nanorod metasurfaces. In both cases, the input is LCP (left) and RCP (right), and the magnetic field is normalized to the impinging amplitude.

curves intersect with a phase difference of 83° instead of 90°. Still, the performance in terms of DOLP and AOLP is pretty robust. Obviously, a new design considering the substrate presence may further improve the overall functionality.

Finally, Fig. 6 shows the distribution of the normal component of the magnetic field distribution (snapshot in time, normalized to the impinging transverse field) at the design frequency at the output of the two considered metasurfaces [nanoslit, Fig. 6(a), and nanorod, Fig. 6(b)] for circularly polarized excitation at normal incidence. The two plots in each panel correspond to LCP (left) and RCP (right) inputs. It is seen how the two excitations provide similar phase distributions around the inclusions, indicating typically dipolar polarizations for both orthogonal elements, which are in phase or out of phase with each other depending on the circularly polarized input. We have sketched in Fig. 6 the dipolar response of each rod, which confirms the nanoscale physical mechanism behind the operation as an ultrathin quarter-wave plate. Indeed, for a circular polarization input, which is formed by two linear polarizations 90° out of phase, the metausrface inclusions are polarized in phase, ensuring linearly polarized transmitted and reflected fields. On purpose, we show here the *normal* component of the magnetic fields, which allows isolating the metasurface response without interfering with the purely tangential excitation fields.

## IV. CONCLUSIONS

We have investigated here the functionality and design of plasmonic metasurfaces formed by orthogonal elongated nanorods and complementary nanoslits to realize ultrathin quarter-wave plates. Based on a simple impedance model to describe the array interaction, we have achieved polarization control of the impinging light and optimized its bandwidth of operation. Our full-wave simulations confirm the expected response and show a rather robust performance in terms of incidence angle and bandwidth of operation. Practical integration of these designs within optical sensors and cameras will be explored in future presentations to realize polarizers and sensors for circularly polarized light.

## ACKNOWLEDGMENTS

This work has been supported by an AFOSR YIP Grant No. FA9550-11-1-0009, an NSF CAREER Award No. ECCS-0953311, and an ONR MURI Grant No. N00014-10-1-0942.

*alu@mail.utexas.edu

[1] Y. H. Huang, Y. Zhou, and S. T. Wu, Opt. Express **15**, 6414 (2007).
[2] V. Gruev, R. Perkins, and T. York, Opt. Express **18**, 19087 (2010).
[3] N. Yu, P. Genevet, M. A. Kats, F. Aieta, J.-P. Tetienne, F. Capasso, and Z. Gaburro, Science **334**, 333 (2011).
[4] P. Biagioni, J. S. Huang, L. Duo, M. Finazzi, and B. Hecht, Phys. Rev. Lett. **102**, 256801 (2009).
[5] E. H. Khoo, E. P. Li, and K. B. Crozier, Opt. Lett. **36**, 2498 (2011).
[6] A. Pors, M. G. Nielsen, G. Della Valle, M. Willatzen, O. Albrektsen, and S. I. Bozhevolnyi, Opt. Lett. **36**, 1626 (2011).
[7] A. Drezet, C. Genet, and T. W. Ebbesen, Phys. Rev. Lett. **101**, 043902 (2008).
[8] T. Li, H. Liu, S. M. Wang, X. G. Yin, F. M. Wang, S. N. Zhu, and X. A. Zhang, Appl. Phys. Lett. **93**, 021110 (2008).
[9] F. I. Baida, M. Boutria, R. Oussaid, and D. Van Labeke, Phys. Rev. B **84**, 035107 (2011).
[10] S.-Y. Hsu, K.-L. Lee, E.-H. Lin, M.-C. Lee, and P.-K. Wei, Appl. Phys. Lett. **95**, 013105 (2009).
[11] B. Bai, Y. Svirko, J. Turunen, and T. Vallius, Phys. Rev. A **76**, 023811 (2007).
[12] W.-X. Huang, Y. Zhang, X.-M. Tang, L.-S. Cai, J.-W. Zhao, L. Zhou, Q.-J. Wang, C.-P. Huang, and Y.-Y. Zhu, Opt. Lett. **36**, 3359 (2011).
[13] J. K. Gansel, M. Thiel, M. S. Rill, M. Decker, K. Bade, V. Saile, G. von Freymann, S. Linden, and M. Wegener, Science **325**, 1513 (2009).
[14] A. Alù and N. Engheta, in *Structured Surfaces as Optical Metamaterials*, edited by A. A. Maradudin (Cambridge University Press, Cambridge, 2011).
[15] M. Beruete, M. Sorolla, R. Marques, J. D. Baena, and M. Freire, Electromagnetics **26**, 247 (2006).
[16] C. L. Holloway, M. A. Mohamed, E. F. Kuester, and A. Dienstfrey, IEEE Trans. Electromagn. Compat. **47**, 853 (2005).
[17] O. Luukkonen, C. Simovski, G. Granet, G. Goussetis, D. Lioubtchenko, A. V. Raisanen, and S. A. Tretyakov, IEEE Trans. Antennas Propag. **56**, 1624 (2008).
[18] Y. Zhao, N. Engheta, and A. Alù, Metamaterials **5**, 90 (2011).
[19] A. Alù, A. Salandrino, and N. Engheta, J. Opt. Soc. Am. B **24**, 3014 (2007).
[20] N. Engheta, A. Salandrino, and A. Alu, Phys. Rev. Lett. **95**, 095504 (2005).
[21] C. F. Bohren and D. R. Huffman, *Absorption and Scattering of Light by Small Particles* (Wiley, New York, 1983).
[22] P. A. Belov, S. I. Maslovski, K. R. Simovski, and S. A. Tretyakov, Tech. Phys. Lett. **29**, 718 (2003).

[23]R. Marques, F. Mesa, J. Martel, and F. Medina, IEEE Trans. Antennas Propag. **51**, 2572 (2003).
[24]E. Plum, X.-X. Liu, V. A. Fedotov, Y. Chen, D. P. Tsai, and N. I. Zheludev, Phys. Rev. Lett. **102**, 113902 (2009).
[25]M. Born and E. Wolf, *Principles of Optics*, 7th ed. (Cambridge University Press, New York, 1999).
[26]CST of America, Inc., CST MICROWAVE STUDIO, Framingham, MA, 2010.
[27]P. B. Johnson and R. W. Christy, Phys. Rev. B **6**, 4370 (1972).
[28]F. Falcone, T. Lopetegi, M. A. G. Laso, J. D. Baena, J. Bonache, M. Beruete, R. Marqués, F. Martín, and M. Sorolla, Phys. Rev. Lett. **93**, 197401 (2004).
[29]C. Rockstuhl, T. Zentgraf, T. P. Meyrath, H. Giessen, and F. Lederer, Opt. Express **16**, 2080 (2008).
[30]T. Zentgraf, T. P. Meyrath, A. Seidel, S. Kaiser, H. Giessen, C. Rockstuhl, and F. Lederer, Phys. Rev. B **76**, 033407 (2007).
[31]H. Raether, *Surface Plasmons on Smooth and Rough Surfaces and on Gratings* (Springer, Berlin, 1988).
[32]D. H. Dawes, R. C. McPhedran, and L. B. Whitbourn, Appl. Opt. **28**, 3498 (1989).